YONGHAO GUI, XIONGFEI WANG, FREDE BLAABJERG, and DONGHUA PAN

This article discusses the mathematical relationship between grid-voltage-modulated (GVM) direct-power control (DPC) and vector-current control (VCC) for three-phase voltage-source converters (VSCs). GVM-DPC is equivalent to VCC at the steady state, and it presents a superior transient performance by removing the need for the phase-locked loop (PLL). This means that GVM-DPC solves the disadvantage of conventional DPC, such as poor steady-state performance. Moreover, GVM-DPC will reduce the computational burden in comparison with VCC due to the absence of Park transformation and PLL. Consequently, we can expect that the GVM-DPC method will be capable of plug-and-play for VSCs. Finally, the experimental results match the theoretical expectations closely.

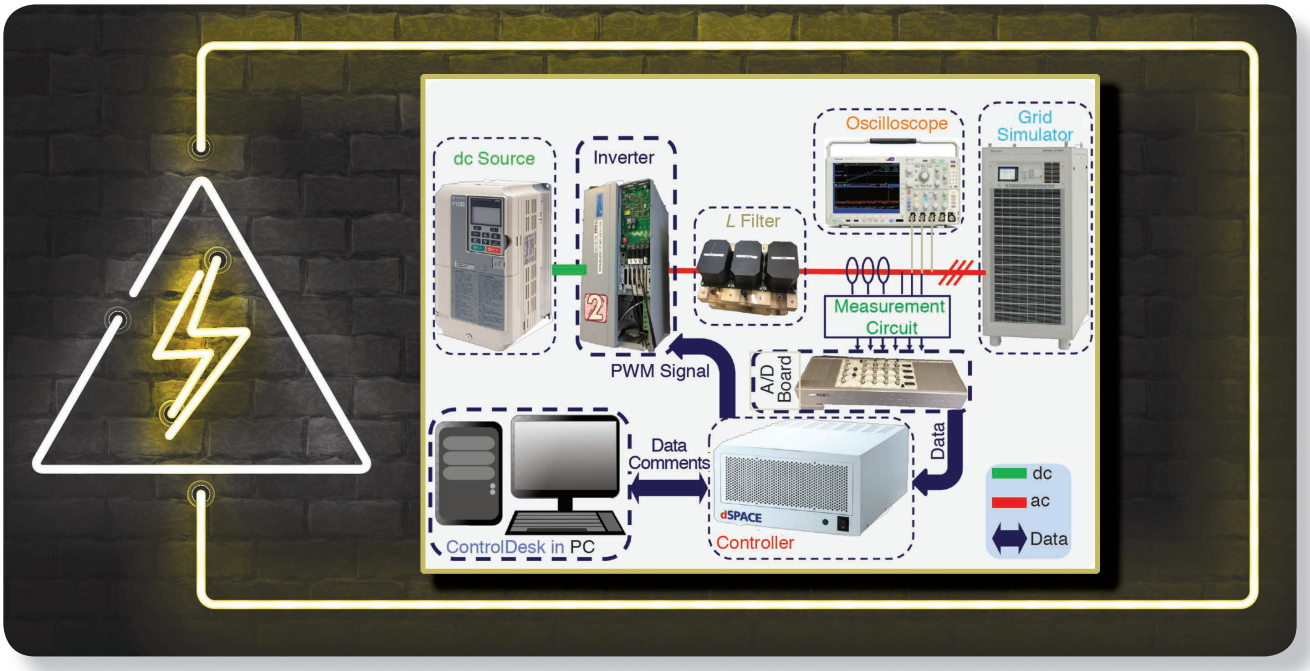

BACKGROUND —©ISTOCKPHOTO.COM/COMIC SANS

Control of Grid-Connected Voltage-Source Converters

The Relationship Between Direct-Power Control and Vector-Current Control

Digital Object Identifier 10.1109/MIE.2019.2898012
Date of publication: 25 June 2019

VSCs are widely used in the application of smart grids, flexible ac transmission systems, and renewable energy sources (e.g., wind and solar).

Control of Grid-Connected VSCs

VSCs are widely used in the application of smart grids, flexible ac transmission systems, and renewable energy sources (e.g., wind and solar) [1]–[6]. Various control methods have been researched for VSCs to improve their performance, stability, and robustness [7].

The conventional control of a grid-connected VSC uses VCC, which is designed in a synchronously rotating reference frame, and a proportional integral (PI) control with a decoupling term is applied to control *d*- and *q*-axis currents independently [8]. It uses coordinate transformation to transform the ac components to dc, and, thus, the linear PI controller can be used. Moreover, the VSC system is changed to a linear-time-invariant (LTI) system in the rotating reference frame, which means that the system can be readily designed and analyzed through linear control techniques [9]–[11]. The main disadvantage of the conventional VCC is that it suffers from a slow transient response, because it uses a PLL system for the coordinate transformation. In addition, the interaction between the PLL and current loop control systems causes harmonic problems in a weak grid and can even destabilize the system [12]–[15].

An alternative control strategy, the direct torque control (DTC), has emerged for induction machine drives [16], [17], and it has a simple structure in comparison with VCC. To achieve the constant switching frequency, a modified DTC strategy based on space vector modulation was developed [18], [19]. Based on the DTC strategy concept, the DPC was created for grid-connected VSCs [20]–[22]. In [20] and [21], a lookup table (LUT) DPC was formulated in which the proper switching states are selected from a predefined optimal switching table based on the instantaneous errors of active and reactive powers and the angular position of the VSC terminal voltage. However, the variable switching frequency results in broadband harmonic spectra, which complicates the design of line filters. To solve such a problem, various DPC algorithms were developed for a constant switching frequency [23], [24].

In addition, for robust control, the sliding-mode control (SMC) [25] and passivity-based control (PBC) DPC [26] have been reported to obtain a faster transient response than the PI controller and a better robustness to parameter uncertainties than the LUT-DPC. However, there are still large ripples in both active and reactive powers. Another control strategy, model-predictive control DPC, has good closed-loop behavior with consideration of the system constraints [27], [28]. However, an incorrect voltage sequence selection could affect its performance [29]. Recently, GVM-DPC was introduced in [30] to design a robust but simple control law for not only the convergence rate of the instantaneous active and reactive powers but also the steady-state performance of the VSC, especially reducing the power ripples and total harmonics distortion (THD) of the output current compared with SMC-DPC and PBC-DPC. Another advantage of GVM-DPC is that it converts the original nonlinear system into an LTI system, which can easily be analyzed and designed by using conventional linear control techniques [31]. In [32], Gui et al. proposed a novel VCC method based on the concept of GVM-DPC.

Although GVM-DPC shows a better steady-state performance than SMC-DPC and PBC-DPC, there has been no analysis to explain how and why this is so. This article presents a detailed comparison of GVM-DPC and conventional VCC designed in the *d-q* frame for a three-phase VSC. We mathematically prove that the DPC model of the VSC is equal to the current model in the *d-q* frame, which shows that GVM-DPC is equivalent to VCC at the steady state, yet it has superior transient performance because it removes the PLL. This means that the GVM-DPC method could achieve the same property of steady-state performance as VCC but better tracking performance because there is no PLL. In addition, the GVM-DPC method will reduce computational burden compared with VCC because there is no Park transformation or PLL system. Consequently, the GVM-DPC method could be applied to various applications and be modified to solve various industry issues.

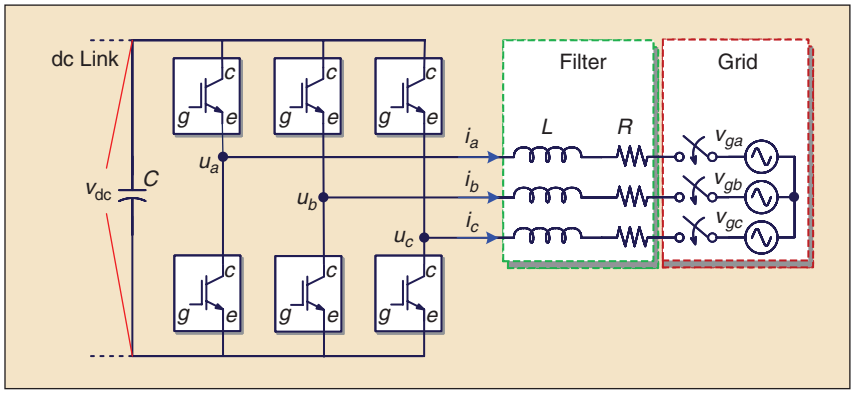

FIGURE 1 – A grid-connected two-level VSC with an *L* filter.

GVM-DPC

In this section, a model of the VSC in the stationary reference frame is described. Then, the DPC modeling of a VSC is briefly introduced. For the VSC system, GVM-DPC is designed to be an LTI multiple-input, multiple-output (MIMO) system.

Modeling VCC

Figure 1 shows a simplified circuit of a two-level VSC connected to the grid with an L filter. The dc side could be connected to renewable energy sources or energy storage systems with a capacitor C. The relationship among the VSC output voltages, the grid voltages, and the output currents can be expressed as

$$\begin{aligned} u_a &= Ri_a + L\frac{di_a}{dt} + v_{ga} \\ u_b &= Ri_b + L\frac{di_b}{dt} + v_{gb} \\ u_c &= Ri_c + L\frac{di_c}{dt} + v_{gc}, \end{aligned} \tag{1}$$

where $v_{ga,b,c}$, $i_{a,b,c}$, and $u_{a,b,c}$ are the three phases of grid voltage, input current, and VSC voltage, respectively. L and R are the filter inductance and resistance, respectively. The Clark transformation is defined as [33]

$$T_{abc2\alpha\beta} = \frac{2}{3}\begin{bmatrix} 1 & -\frac{1}{2} & -\frac{1}{2} \\ 0 & -\frac{\sqrt{3}}{2} & -\frac{\sqrt{3}}{2} \end{bmatrix}. \tag{2}$$

Based on a balanced grid voltage condition, the relationship in (1) can be expressed in the stationary reference frame by using the Clark transformation in (2) as [34]

$$\begin{aligned} u_\alpha &= Ri_\alpha + L\frac{di_\alpha}{dt} + v_{g\alpha} \\ u_\beta &= Ri_\beta + L\frac{di_\beta}{dt} + v_{g\beta}, \end{aligned} \tag{3}$$

where $v_{g\alpha}$ and $v_{g\beta}$ indicate the grid voltages, i_α and i_β are the output currents, and u_α and u_β represent the VSC output voltages in the α-β frame. Then, we give the Park transformation.

$$T_{\alpha\beta 2dq} = \begin{bmatrix} \cos(\theta) & \sin(\theta) \\ -\sin(\theta) & \cos(\theta) \end{bmatrix}, \tag{4}$$

where θ is a phase angle, usually calculated by using PLL. In this study, the d-axis is always coincident with the instantaneous voltage vector, and the q-axis is in quadrature with it; that is, $v_{gd} = V_g$ and $v_{gq} = 0$. By using the Park transformation in (4), the current model (3) can be presented in the d-q frame as [33]

The interaction between the PLL and current loop control systems causes harmonic problems in a weak grid and can even destabilize the system.

$$\begin{aligned} L\frac{di_d}{dt} &= -Ri_d + L\omega i_q + u_d - v_{gd} \\ L\frac{di_q}{dt} &= -L\omega i_d - Ri_q + u_q, \end{aligned} \tag{5}$$

where v_{gd} and v_{gq} indicate the grid voltages, i_d and i_q indicate the output currents, and u_d and u_q indicate the VSC output voltages in the d-q frame. ω is the angular frequency of the grid voltage, and $\omega = 2\pi f$, where f is the frequency of the grid voltage.

Modeling DPC

We define the instantaneous active and reactive powers of the VSC in the stationary reference frame as [34]

$$\begin{aligned} P &= \frac{3}{2}(v_{g\alpha}i_\alpha + v_{g\beta}i_\beta) \\ Q &= \frac{3}{2}(v_{g\beta}i_\alpha - v_{g\alpha}i_\beta), \end{aligned} \tag{6}$$

where P and Q are the active and reactive powers of the VSC, respectively. We can express the instantaneous active and reactive power variation based on the grid voltages and output currents variation by differentiating (6):

$$\begin{aligned} \frac{dP}{dt} &= \frac{3}{2}\left(i_\alpha\frac{dv_{g\alpha}}{dt} + v_{g\alpha}\frac{di_\alpha}{dt} + i_\beta\frac{dv_{g\beta}}{dt} + v_{g\beta}\frac{di_\beta}{dt}\right) \\ \frac{dQ}{dt} &= \frac{3}{2}\left(i_\alpha\frac{dv_{g\beta}}{dt} + v_{g\beta}\frac{di_\alpha}{dt} - i_\beta\frac{dv_{g\alpha}}{dt} - v_{g\alpha}\frac{di_\beta}{dt}\right). \end{aligned} \tag{7}$$

In this study, we consider a nondistorted grid. Thus, we can obtain the following relationship,

$$\begin{aligned} v_{g\alpha} &= V_g\cos(\omega t) \\ v_{g\beta} &= V_g\sin(\omega t), \end{aligned} \tag{8}$$

where v_g is the amplitude of the grid voltage. Then, the instantaneous grid voltage variations can be obtained by differentiating (8):

$$\begin{aligned} \frac{dv_{g\alpha}}{dt} &= -\omega V_g\sin(\omega t) = -\omega v_{g\beta} \\ \frac{dv_{g\beta}}{dt} &= \omega V_g\cos(\omega t) = \omega v_{g\alpha}. \end{aligned} \tag{9}$$

Substituting (3) and (9) into (7), we can obtain a state-space model of the active and reactive powers:

$$\begin{aligned} \frac{dP}{dt} &= -\frac{R}{L}P - \omega Q + \frac{3}{2L}(v_{g\alpha}u_\alpha + v_{g\beta}u_\beta - V_g^2) \\ \frac{dQ}{dt} &= \omega P - \frac{R}{L}Q + \frac{3}{2L}(v_{g\beta}u_\alpha - v_{g\alpha}u_\beta). \end{aligned} \tag{10}$$

Modeling GVM-DPC

As represented in (10), the dynamics of the VSC with an L filter is a time-varying MIMO system. In [30], the GVM control inputs are defined to decouple the outputs from the two inputs as

$$\begin{bmatrix} u_P \\ u_Q \end{bmatrix} = \begin{bmatrix} v_{g\alpha}u_\alpha + v_{g\beta}u_\beta \\ -v_{g\beta}u_\alpha + v_{g\alpha}u_\beta \end{bmatrix}. \tag{11}$$

Based on (8), the new GVM control inputs (11) can be represented in the d-q frame as

$$\begin{aligned} \begin{bmatrix} u_P \\ u_Q \end{bmatrix} &= V_g\underbrace{\begin{bmatrix} \cos(\omega t) & \sin(\omega t) \\ -\sin(\omega t) & \cos(\omega t) \end{bmatrix}}_{\text{Park Transformation}}\begin{bmatrix} u_\alpha \\ u_\beta \end{bmatrix} \\ &= V_g\begin{bmatrix} u_d \\ u_q \end{bmatrix}. \end{aligned} \tag{12}$$

Based on (12), the original system (10) can be represented as

$$\begin{aligned} \frac{dP}{dt} &= -\frac{R}{L}P - \omega Q + \frac{3}{2L}(u_P - V_g^2) \\ \frac{dQ}{dt} &= \omega P - \frac{R}{L}Q - \frac{3}{2L}u_Q. \end{aligned} \tag{13}$$

GVM-DPC presents the system in the d-q frame without using the PLL. Notice that (13) is converted into an LTI system with some coupling states. Consequently, it can be easily analyzed and designed by using conventional linear control techniques [31].

Relationship Between DPC and VCC

In this section, we show a relationship between GVM-DPC and conventional VCC designed in a synchronous rotating frame. Then, we compare the conventional VCC and GVM-DPC methods.

Relationship Between GVM-DPC and VCC

Since the system in (5) is defined where the d-axis is always coincident with the instantaneous voltage vector and the q-axis is in quadrature with it, $v_{gd} = V_g$ and $v_{gq} = 0$. Consequently, the active and reactive powers in the d-q frame can be defined as

$$P = \frac{3}{2} V_g i_d$$
$$Q = -\frac{3}{2} V_g i_q. \tag{14}$$

If we multiply $(2/3V_g)$ to both sides of (13), a new system can be obtained:

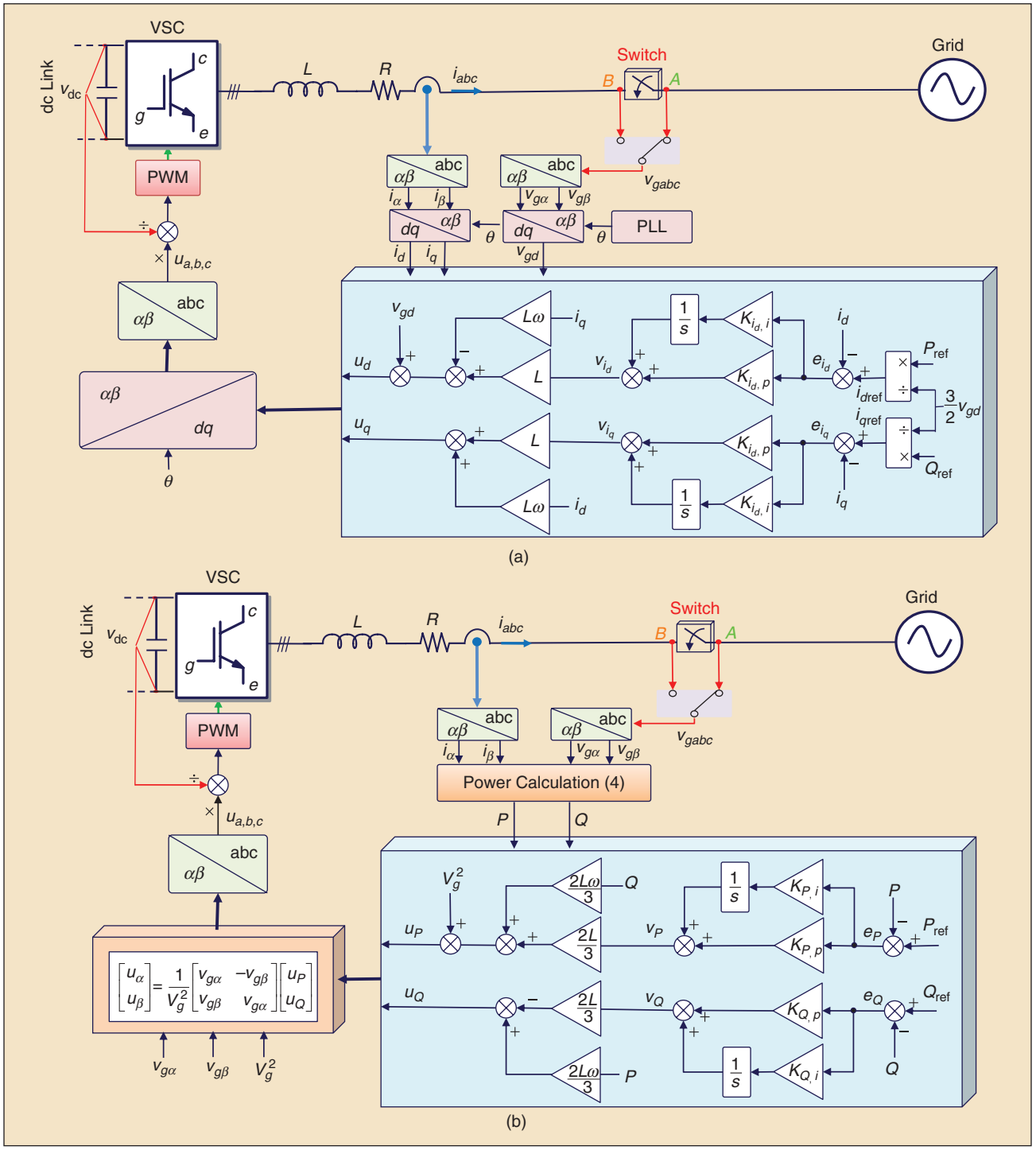

FIGURE 2 – A block diagram of (a) conventional VCC and (b) GVM-DPC. PWM: pulsewidth modulation.

$$\frac{di_d}{dt} = -\frac{R}{L} i_d + \omega i_q + \frac{1}{L}(u_d - V_g)$$
$$\frac{di_q}{dt} = -\omega i_d - \frac{R}{L} i_q + \frac{1}{L} u_q. \quad (15)$$

It is obvious that the DPC model is changed into a conventional *d-q* current model. Consequently, we can achieve zero steady-state error by using a PI controller, which is the same as VCC. In contrast, we can expect that a controller designed based on (13) will obtain a faster transient response because there is no need for the PLL.

VCC Designed in the d-q *Frame*

In this article, we show only a traditional controller, consisting of feedforward and feedback to regulate *d*- and *q*-axis currents. First, we define errors of the *d-q*–axis currents as

$$e_{i_d} = i_{\text{dref}} - i_d$$
$$e_{i_q} = i_{\text{qref}} - i_q, \quad (16)$$

where i_{dref} and i_{qref} are *d-q*–axis currents references, respectively. A controller consisting of feedforward and feedback is designed as [35]

$$u_d = \underbrace{V_g - L\omega i_q}_{\text{feedforward}} + \underbrace{L v_{i_d}}_{\text{feedback}}$$
$$u_q = \underbrace{L\omega i_d}_{\text{feedforward}} + \underbrace{L v_{i_q}}_{\text{feedback}}, \quad (17)$$

where v_{i_d} and v_{i_q} are the feedback control inputs. To obtain zero steady-state error, a PI controller is applied to v_{i_d} and v_{i_q},

$$v_{i_d} = K_{i_d,p} e_{i_d} + K_{i_d,i} \int_0^t e_{i_d}(\tau)\, d\tau$$
$$v_{i_q} = K_{i_q,p} e_{i_q} + K_{i_q,i} \int_0^t e_{i_q}(\tau)\, d\tau, \quad (18)$$

where $K_{i_d,p}$, $K_{i_d,i}$, $K_{i_q,p}$, and $K_{i_q,i}$ are the PI controller gains. For the PI controller gain design, substituting from (16) to (18) into (15), a closed-loop system can be obtained, such as

$$\frac{di_d}{dt} = -\frac{R}{L} i_d + K_{i_d,p}(i_{\text{dref}} - i_d) + K_{i_d,i} \int (i_{\text{dref}} - i_d)\, dt$$
$$\frac{di_q}{dt} = -\frac{R}{L} i_1 + K_{i_q,p}(i_{\text{qref}} - i_q) + K_{i_q,i} \int (i_{\text{qref}} - i_q)\, dt. \quad (19)$$

If we differentiate (19), it is changed to a second-order system:

$$\frac{d^2 i_d}{dt^2} = -\frac{R}{L}\frac{di_d}{dt} + K_{i_d,p}\frac{d(i_{\text{dref}} - i_d)}{dt} + K_{i_d,i}(i_{\text{dref}} - i_d)$$
$$\frac{d^2 i_q}{dt^2} = -\frac{R}{L}\frac{di_q}{dt} + K_{i_q,p}\frac{d(i_{\text{qref}} - i_q)}{dt} + K_{i_q,i}(i_{\text{qref}} - i_q). \quad (20)$$

Applying the Laplace transform to (20) yields

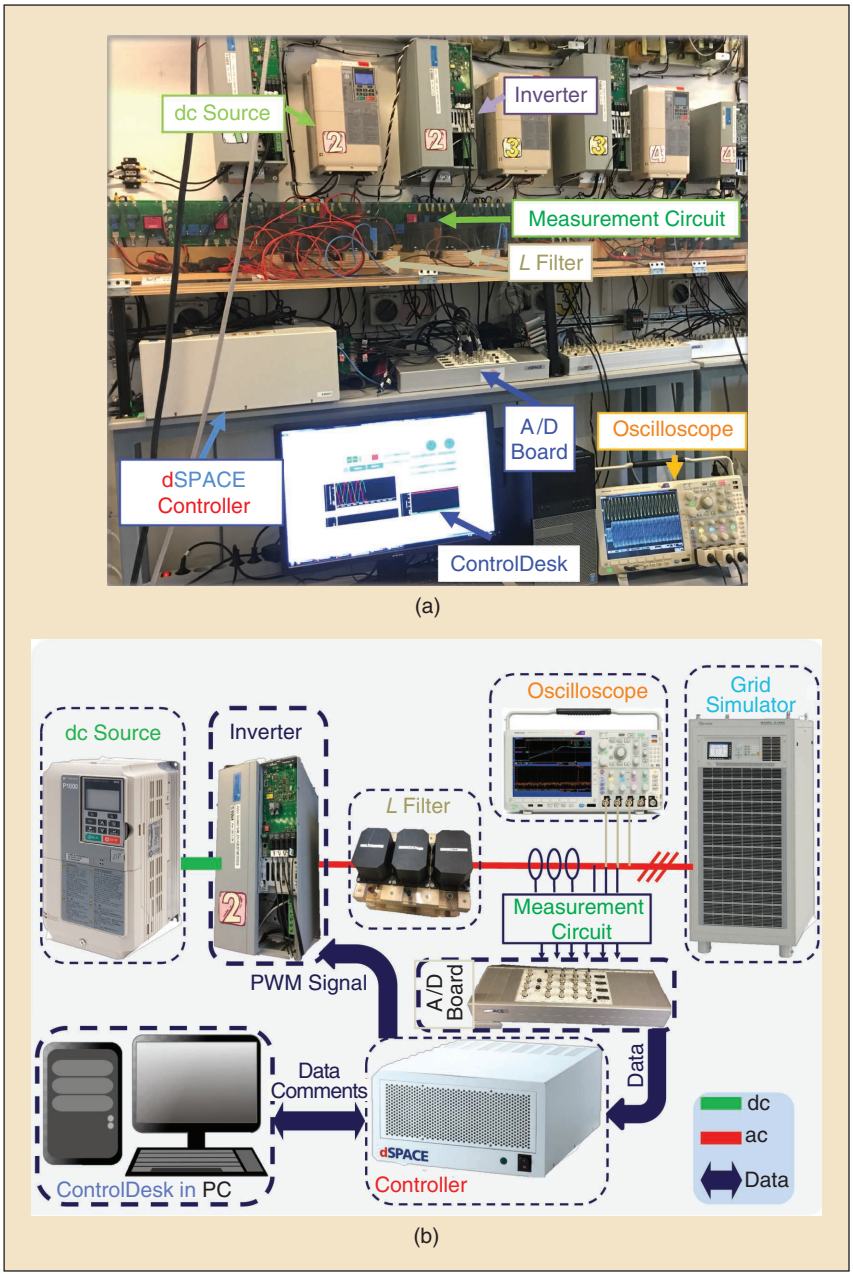

FIGURE 3 – (a) An experimental test setup in the laboratory at Aalborg University. (b) The configuration of the setup. A/D: analog to digital.

TABLE 1 – SYSTEM PARAMETERS USED IN SIMULATION.

PARAMETER	VALUE
Nominal bus voltage, V_{rms}	110 V
Nominal bus frequency, f	50 Hz
Filter inductance, L	5 mH
Filter resistance, R	0.2 Ω
Switching frequency, f_{sw}	10 kHz
Sampling period, T_s	0.1 ms

$$
\begin{aligned}
s^2 i_d &= -\frac{R}{L} s i_d + K_{i_d,p} s (i_{\text{dref}} - i_d) \\
&\quad + K_{i_d,i} (i_{\text{dref}} - i_d) \\
s^2 i_q &= -\frac{R}{L} s i_q + K_{i_q,p} s (i_{\text{qref}} - i_q) \\
&\quad + K_{i_q,i} (i_{\text{qref}} - i_q)
\end{aligned} \tag{21}
$$

or, equivalently,

$$
\begin{aligned}
\frac{i_d(s)}{i_{\text{dref}}(s)} &= \frac{K_{i_d,p} s + K_{i_d,i}}{s^2 + \left(K_{i_d,p} + \frac{R}{L}\right) s + K_{i_d,i}}, \\
\frac{i_q(s)}{i_{\text{qref}}(s)} &= \frac{K_{i_q,p} s + K_{i_q,i}}{s^2 + \left(K_{i_q,p} + \frac{R}{L}\right) s + K_{i_q,i}}.
\end{aligned} \tag{22}
$$

The PI controller gains could be selected based on the traditional second-order system in (21) [36].

Controller Design for GVM-DPC

In this section, a conventional controller, including feedforward and feedback, is designed to make the active and reactive powers track their references. Errors of the active and reactive powers are defined as

$$
\begin{aligned}
e_P &= P_{\text{ref}} - P \\
e_Q &= Q_{\text{ref}} - Q,
\end{aligned} \tag{23}
$$

where P_{ref} and Q_{ref} are the active and reactive power references, respectively. To compare with conventional VCC fairly, we design the same control structure as in the d-q frame. To cancel the coupling terms, we take a control law with a feedforward and feedback, such as

$$
\begin{aligned}
u_P &= \underbrace{V_g^2 + \frac{2L\omega}{3} Q}_{\text{feedforward}} + \underbrace{\frac{2L}{3} \nu_P}_{\text{feedback}} \\
u_Q &= \underbrace{\frac{2L\omega}{3} P}_{\text{feedforward}} - \underbrace{\frac{2L}{3} \nu_Q}_{\text{feedback}},
\end{aligned} \tag{24}
$$

where ν_P and ν_Q are the feedback control inputs. To obtain zero steady-state error, the PI controller is applied to ν_P and ν_Q

$$
\begin{aligned}
\nu_P &= K_{P,p} e_P + K_{P,i} \int_0^t e_P(\tau) d\tau \\
\nu_Q &= K_{Q,p} e_Q + K_{Q,i} \int_0^t e_Q(\tau) d\tau,
\end{aligned} \tag{25}
$$

where $K_{P,p}, K_{P,i}, K_{Q,p}$, and $K_{Q,i}$ are the PI controller gains. Finally, the original control inputs can be calculated based on the inverse of (11).

If we use controller gains as positive values, the system is globally exponentially stable [37]. For the controller gain design, by substituting from (23) to (25) into (13), a closed-loop system is obtained

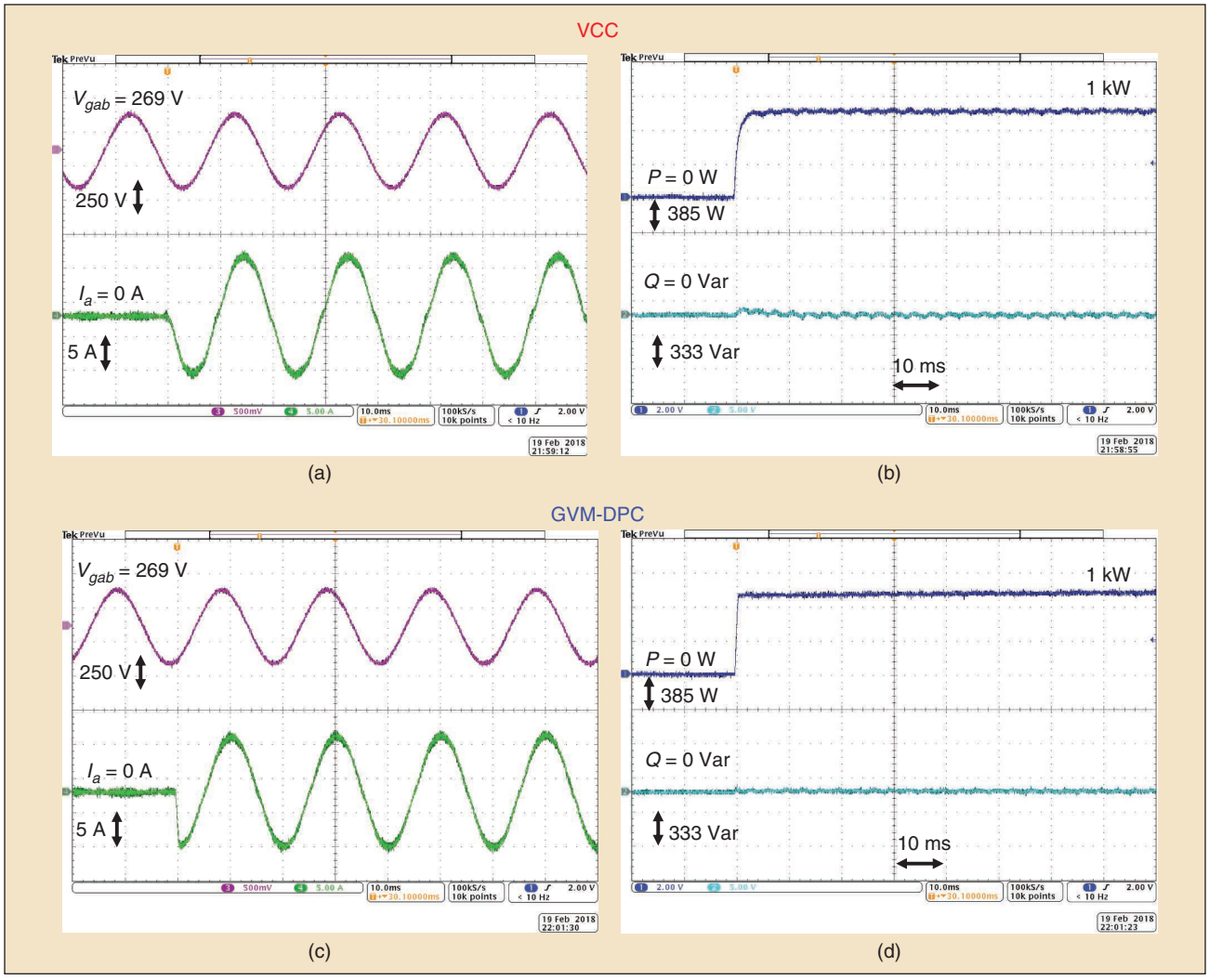

FIGURE 4 – The experimental results when the active power step changes. VCC: (a) the line-to-line grid voltage (V_{gab}) and current (I_a) and (b) the active and reactive powers. GVM-DPC: (c) the line-to-line grid voltage (V_{gab}) and current (I_a) and (d) the active and reactive powers.

$$\frac{dP}{dt} = -\frac{R}{L}P + K_{P,p}(P_{\text{ref}} - P) + K_{P,i}\int (P_{\text{ref}} - P)\,dt$$
$$\frac{dQ}{dt} = -\frac{R}{L}Q + K_{Q,p}(Q_{\text{ref}} - Q) + K_{Q,i}\int (Q_{\text{ref}} - Q)\,dt. \quad (26)$$

If we differentiate (26), then it is changed to a second-order system as

$$\frac{d^2P}{dt^2} = -\frac{R}{L}\frac{dP}{dt} + K_{P,p}\frac{d(P_{\text{ref}} - P)}{dt} + K_{P,i}(P_{\text{ref}} - P)$$
$$\frac{d^2Q}{dt^2} = -\frac{R}{L}\frac{dQ}{dt} + K_{Q,p}\frac{d(Q_{\text{ref}} - Q)}{dt} + K_{Q,i}(Q_{\text{ref}} - Q). \quad (27)$$

Applying the Laplace transform to (27) yields

$$s^2P = -\frac{R}{L}sP + K_{P,p}s(P_{\text{ref}} - P) + K_{P,i}(P_{\text{ref}} - P)$$
$$s^2Q = -\frac{R}{L}sQ + K_{Q,p}s(Q_{\text{ref}} - Q) + K_{Q,i}(Q_{\text{ref}} - Q), \quad (28)$$

or, equivalently,

$$\frac{P(s)}{P_{\text{ref}}(s)} = \frac{K_{P,p}s + K_{P,i}}{s^2 + \left(K_{P,p} + \frac{R}{L}\right)s + K_{P,i}}$$
$$\frac{Q(s)}{Q_{\text{ref}}(s)} = \frac{K_{Q,p}s + K_{Q,i}}{s^2 + \left(K_{Q,p} + \frac{R}{L}\right)s + K_{Q,i}}. \quad (29)$$

Figure 2(b) shows the block diagram of the GVM-DPC method. Both the VCC and GVM-DPC methods consist of a similar structure with the feedforward and PI feedback. The GVM-DPC method has only the power calculation (6) and the original input calculation, whereas VCC includes PLL, the Park transformation, and the inverse Park transformation. Consequently, we can conclude that the GVM-DPC method reduces the computational burden.

Controller Gains Tuning

Normally, the PI controller gains of the VCC method are tuned by considering the overall system dynamics, which are evaluated by the crossover frequency ω_c and the phase margin (PM). With consideration of the time delay, which consists of one sampling period (T_s) of computation delay and a half sampling period ($0.5T_s$) of pulsewidth modulation delay [38], ω_c is related to PM by [39]

$$\omega_c = \frac{\pi/2 - PM}{1.5T_s}. \quad (30)$$

Based on ω_c in (30), the proportional gain K_p can be obtained approximately as

$$K_p \approx \omega_c L. \quad (31)$$

To minimize the phase contribution of the PI regulator at ω_c, its corner frequency is usually set a decade below ω_c [40]. Thus, the integral gain K_i can be calculated as

$$K_i = \frac{\omega_c}{10}K_p. \quad (32)$$

Because the GVM-DPC method gets the same closed-loop dynamics as the VCC method, its controller gains can also be calculated based on the aforementioned procedure.

Performance Validation

The effectiveness of the GVM-DPC method is compared with VCC by using a three-leg, three-phase, 15-kVA inverter with an L filter. The control system is implemented by using the DS1007 dSPACE system, where the switching pulses are generated by using the DS5101 digital waveform output board, and the grid voltages and currents are measured by using the DS2004 high-speed analog-to-digital

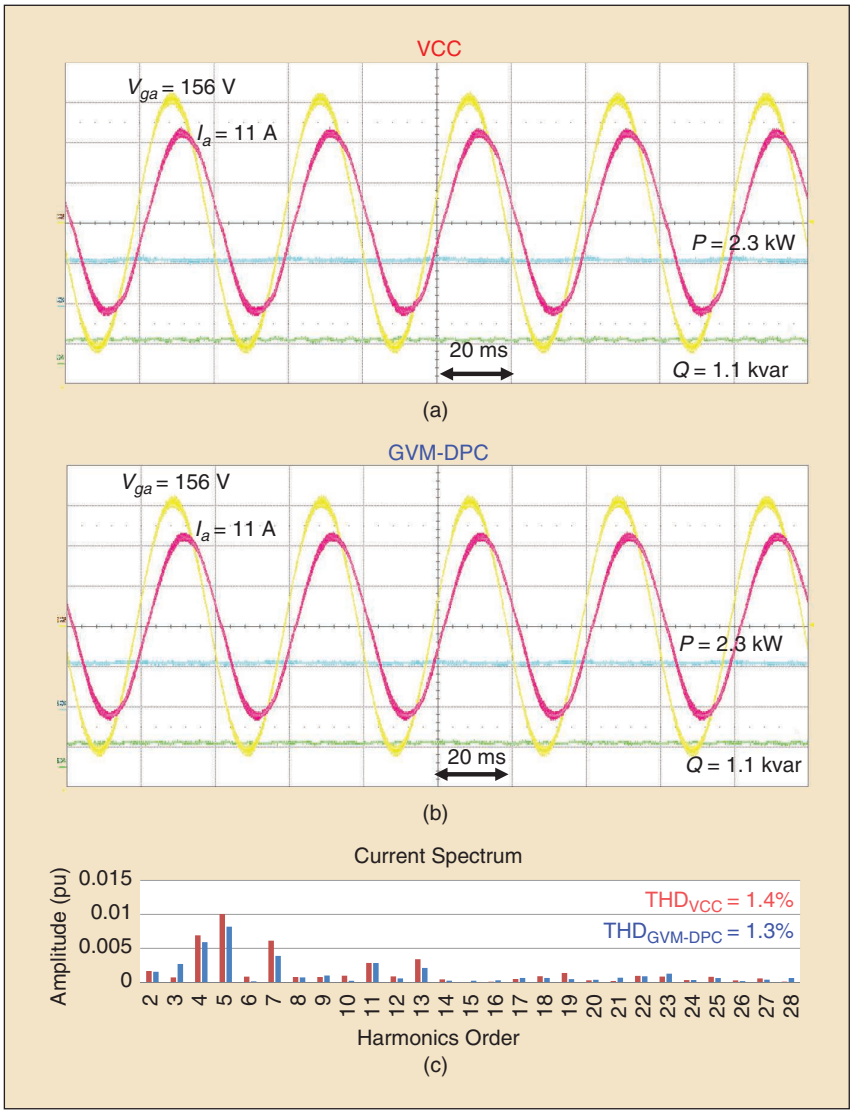

FIGURE 5 – The measured performance of (a) VCC and (b) GVM-DPC when $P = 2.3$ kW and $Q = 1.1$ kvar. (c) The spectrum analysis of the current. Yellow line: grid voltage V_{ga}; pink line: output current I_a; blue line: P; and green line: Q.

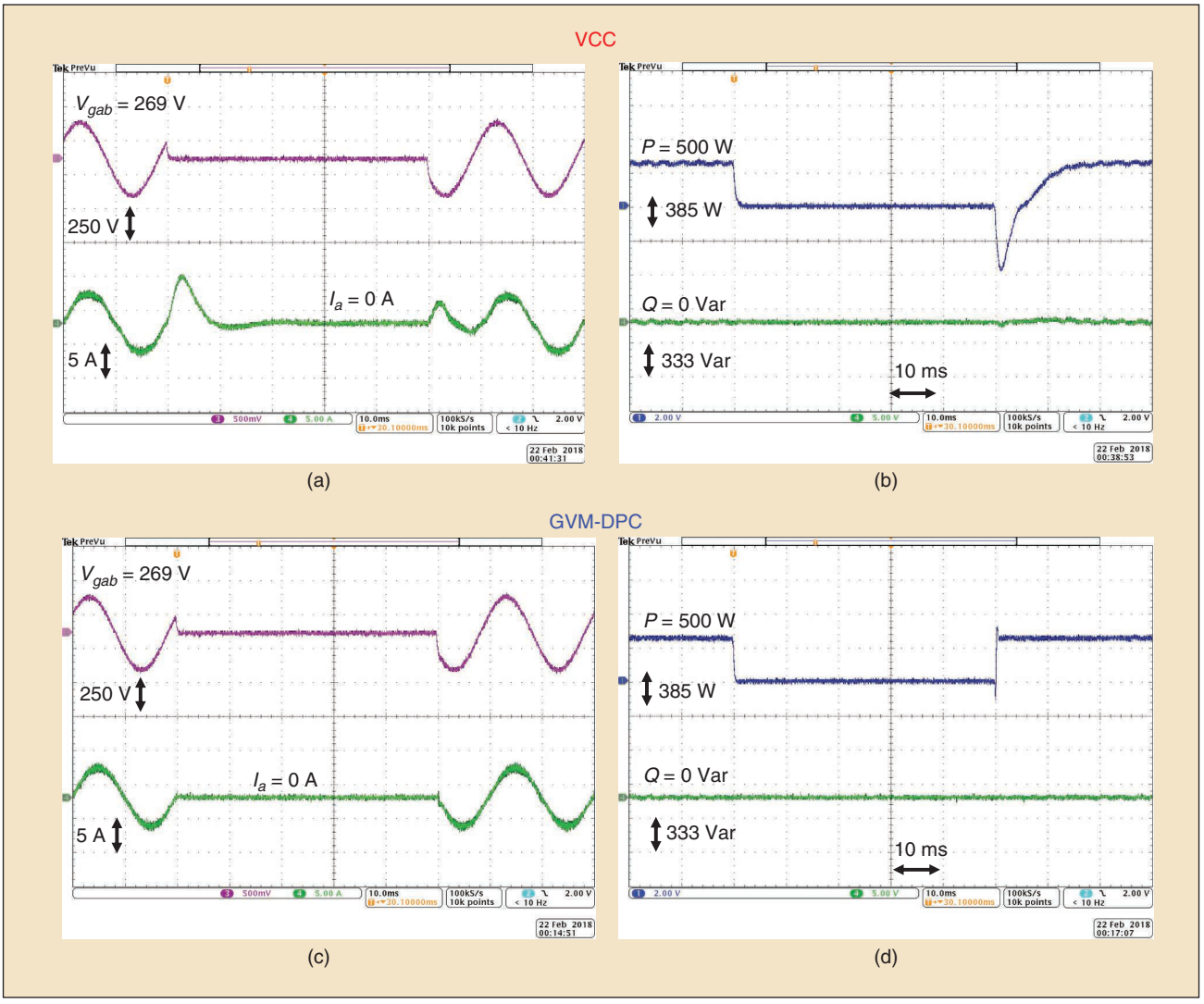

FIGURE 6 – The LVRT performance when the grid has 100% voltage sag. VCC: (a) the line-to-line grid voltage (V_{gab}) and current (I_a) and (b) the active and reactive powers. GVM-DPC: (c) the line-to-line grid voltage (V_{gab}) and current (I_a) and (d) the active and reactive powers.

board. A constant dc voltage supply is used at the dc side. Furthermore, the ac side is connected to a grid simulator, which generates 110 V, as shown in Figure 3. The parameters of the system used in the experimental test are listed in Table 1. In the test, the PM in (30) is set to 45°.

As the first test, the reference of the active power is changed from 0 kW to 1 kW. Figure 4 shows the time response of the VCC and GVM-DPC methods. In this case, the grid voltages are measured at point A in Figure 2 (i.e., the VSC continuously measures the grid voltages even when it is not injecting power, as shown in Figure 4). The main disadvantage of the conventional DPC method is the steady-state performance (i.e., power ripple) compared to the VCC method designed in the *d-q* frame [25], [37]. However, GVM-DPC has a similar active power-tracking performance compared to the VCC method (Figure 4). Moreover, as shown in Figure 5, the THDs of the output current using both methods are similar, because the GVM-DPC method has a same model as that in the *d-q* frame, as discussed in the "GVM-DPC" section. In this case, the PLL system can continually provide the correct information of phase angle; hence, we can conclude that the results in Figure 4 are acceptable.

In addition, we test the robustness of both methods to grid voltage, that is, low-voltage ride-through (LVRT) capability. Figure 6 shows the time response of the VCC and GVM-DPC methods when the grid has a 100% balanced voltage sag. In this case, we set the references as $P_{\text{ref}} = 0.5$ kW and $Q_{\text{ref}} = 0$ kvar and as $P_{\text{ref}} = 0$ kW at the time when the fault happens. The line current with VCC has a large overshoot when the voltage sag occurs. Especially when the grid voltage returns to its nominal value after faults, the active power with the VCC method has a larger overshoot than the GVM-DPC method due to the slow dynamics of the PLL system. However, the trajectory with the GVM-DPC method converges to its new operating point quickly, even at the time when the fault clears. The case in which the grid voltages are measured from 0 to their nominal values can also be found in the module uninterruptible power-supply (UPS) system, which has a hot-swap operation property [41]. This

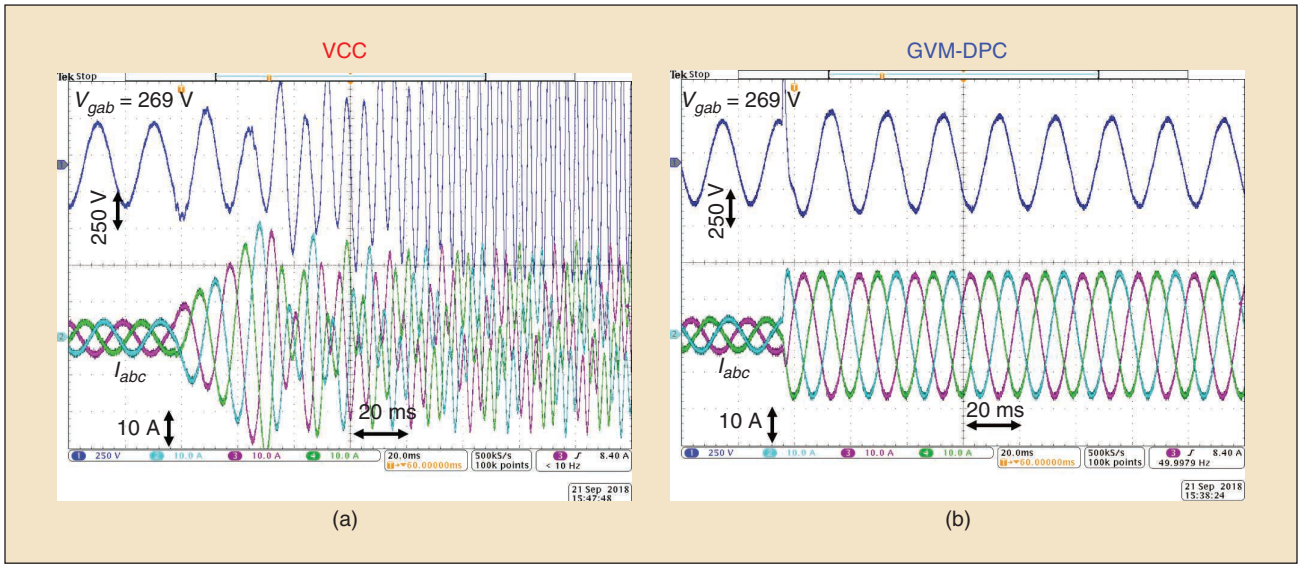

FIGURE 7 – The measured time response of the VSC when the active power is injected to the grid from 0.5 kW to 2 kW. (a) VCC. (b) GVM-DPC.

means that when one UPS module fails, the redundant power modules have to take over immediately to guarantee the electricity supply to the loads. Hence, the redundant power modules do nothing in normal time (that is, the grid voltages are not measured at point B in Figure 2). It can be expected that GVM-DPC has the enhanced capability of plug and play.

Finally, we test both methods in a weak grid, where the frequency and phase shift step and fluctuate [42]. In this case, we use 22 mH $-L$ and 15 μF $-C$ to construct a grid impedance, where the short circuit ratio is 1.5. In Figure 7(a), the VCC method destabilizes the system due to the PLL system, as discussed in [15]. However, the GVM-DPC method can stabilize the system because it eliminates the PLL system, as shown in Figure 7(b). Consequently, we can conclude that GVM-DPC has the same property in the normal cases but that it has good dynamic capabilities in some special cases in which the PLL system can cause problems.

Conclusions

In this article, we presented a relationship between GVM-DPC and VCC designed in a synchronous rotating reference frame for a three-phase VSC. We mathematically showed that GVM-DPC is equal to the current model in the synchronous rotating reference frame. This means that GVM-DPC could achieve the same steady-state performance as VCC but better tracking performance because of PLL elimination in the control method implementation. Furthermore, GVM-DPC will reduce the computational burden in comparison with the synchronous controller because there is neither *d-q* transformation nor a PLL system. Finally, the experimental results show that GVM-DPC has same property in normal cases as VCC but that it has better dynamic capabilities in some special cases in which the PLL system causes problems. In the future, GVM-DPC will be modified for various applications to overcome practical issues.

Biographies

Yonghao Gui (yg@es.aau.dk) earned his B.S. degree in automation from Northeastern University, Shenyang, China, in 2009 and his M.S. and Ph.D. degrees in electrical engineering from Hanyang University, Seoul, South Korea, in 2012 and 2017, respectively. From February 2017 to November 2018, he worked with the Department of Energy Technology, Aalborg University, Denmark, as a postdoctoral researcher. Since December 2018, he has been with the Automation and Control Section in the Department of Electronic Systems, Aalborg University, where he is currently an assistant professor. His research interests include power converter control and control theory. He is a Member of the IEEE.

Xiongfei Wang (xwa@et.aau.dk) earned his Ph.D. degree in energy technology from Aalborg University, Denmark, in 2013. He is currently a professor and research program leader for the electronic power grid infrastructure in the Department of Energy Technology, Aalborg University. He serves as an associate editor for three IEEE journals. He received six IEEE prize paper awards and the IEEE Power Electronics Society Richard M. Bass Outstanding Young Power Electronics Engineer Award in 2018. His research interests include modeling and control of grid-interactive power converters and stability and power quality in power-electronic-based power systems. He is a Senior Member of the IEEE.

Frede Blaabjerg (fbl@et.aau.dk) earned his Ph.D. degree in electrical engineering from Aalborg University, Denmark, in 1995. He was with ABB-Scandia, Randers, Denmark, from 1987 to 1988. He became an assistant professor in 1992, an associate professor in 1996, and a full professor of power electronics and drives in 1998, at Aalborg University. In 2017, he became a VILLUM Investigator. He is honoris causa at University Politehnica Timisoara, Romania, and Tallinn Technical University, Estonia. His research interests include working with power converter control together with industry. He is a Fellow of the IEEE.

Donghua Pan (dop@et.aau.dk) earned his B.S. and Ph.D. degrees in electrical engineering from the Huazhong University of Science and Technology, Wuhan, China, in 2010 and 2015, respectively. Since September 2017, he has been with Aalborg University, Denmark, where he is currently a postdoctoral fellow in the Department of Energy Technology. He received the Outstanding Reviewer Award of *IEEE Transactions on Power Electronics* in 2017 and the Best Paper Award at the 2018 IEEE Southern Power Electronics Conference. His research interests include magnetic integration technique, modeling and control of grid-connected converters, and wide-bandgap power conversion systems. He is a Member of the IEEE.

References

[1] M. Liserre, T. Sauter, and J. Y. Hung, "Future energy systems: Integrating renewable energy sources into the smart power grid through industrial electronics," *IEEE Ind. Electron. Mag.*, vol. 4, no. 1, pp. 18–37, 2010. doi: 10.1109/MIE.2010.935861.

[2] F. Blaabjerg, M. Liserre, and K. Ma, "Power electronics converters for wind turbine systems," *IEEE Trans. Ind. Appl.*, vol. 48, no. 2, pp. 708–719, 2012. doi: 10.1109/TIA.2011.2181290.

[3] S. Kouro, J. I. Leon, D. Vinnikov, and L. G. Franquelo, "Grid-connected photovoltaic systems: An overview of recent research and emerging PV converter technology," *IEEE Ind. Electron. Mag.*, vol. 9, no. 1, pp. 47–61, 2015. doi: 10.1109/MIE.2014.2376976.

[4] Y. Gui, W. Kim, and C. C. Chung, "Passivity-based control with nonlinear damping for type 2 STATCOM systems," *IEEE Trans. Power Syst.*, vol. 31, no. 4, pp. 2824–2833, 2016. doi: 10.1109/TPWRS.2015.2482982.

[5] F. Blaabjerg, Y. Yang, D. Yang, and X. Wang, "Distributed power-generation systems and protection," *Proc. IEEE*, vol. 105, no. 7, pp. 1311–1331, 2017. doi: 10.1109/JPROC.2017.2696878.

[6] X. Guo et al., "Leakage current suppression of three-phase flying capacitor PV inverter with new carrier modulation and logic function," *IEEE Trans. Power Electron.*, vol. 33, no. 3, pp. 2127–2135, 2018. doi: 10.1109/TPEL.2017.2692753.

[7] X. Wang, F. Blaabjerg, M. Liserre, Z. Chen, J. He, and Y. Li, "An active damper for stabilizing power-electronics-based AC systems," *IEEE Trans. Power Electron.*, vol. 29, no. 7, pp. 3318–3329, 2014. doi: 10.1109/TPEL.2013.2278716.

[8] M. Kazmierkowski and L. Malesani, "Current control techniques for three-phase voltage-source PWM converters: A survey," *IEEE Trans. Ind. Electron.*, vol. 45, no. 5, pp. 691–703, Oct. 1998. doi: 10.1109/41.720325.

[9] M. Reyes, P. Rodriguez, S. Vazquez, A. Luna, R. Teodorescu, and J. M. Carrasco, "Enhanced decoupled double synchronous reference frame current controller for unbalanced grid-voltage conditions," *IEEE Trans. Power Electron.*, vol. 27, no. 9, pp. 3934–3943, 2012. doi: 10.1109/TPEL.2012.2190147.

[10] Z. Li, C. Zang, P. Zeng, H. Yu, S. Li, and J. Bian, "Control of a grid-forming inverter based on sliding-mode and mixed H_2/H_∞ control," *IEEE Trans. Ind. Electron.*, vol. 64, no. 5, pp. 3862–3872, 2017. doi: 10.1109/TIE.2016.2636798.

[11] X. Wang, L. Harnefors, and F. Blaabjerg, "Unified impedance model of grid-connected voltage-source converters," *IEEE Trans. Power Electron.*, vol. 33, no. 2, pp. 1775–1787, 2018. doi: 10.1109/TPEL.2017.2684906.

[12] P. Rodríguez, A. Luna, I. Candela, R. Mujal, R. Teodorescu, and F. Blaabjerg, "Multiresonant frequency-locked loop for grid synchronization of power converters under distorted grid conditions," *IEEE Trans. Ind. Electron.*, vol. 58, no. 1, pp. 127–138, 2011. doi: 10.1109/TIE.2010.2042420.

[13] D. Dong, B. Wen, D. Boroyevich, P. Mattavelli, and Y. Xue, "Analysis of phase-locked loop low-frequency stability in three-phase grid-connected power converters considering impedance interactions," *IEEE Trans. Ind. Electron.*, vol. 62, no. 1, pp. 310–321, 2015. doi: 10.1109/TIE.2014.2334665.

[14] B. Wen, D. Boroyevich, R. Burgos, P. Mattavelli, and Z. Shen, "Analysis of DQ small-signal impedance of grid-tied inverters," *IEEE Trans. Power Electron.*, vol. 31, no. 1, pp. 675–687, 2016. doi: 10.1109/TPEL.2015.2398192.

[15] X. Wang and F. Blaabjerg, "Harmonic stability in power electronic based power systems: Concept, modeling, and analysis," *IEEE Trans. Smart Grid*, vol. 10, no. 3, pp. 2858–2870, May 2019. doi: 10.1109/TSG.2018.2812712.

[16] I. Takahashi and T. Noguchi, "A new quick-response and high-efficiency control strategy of an induction motor," *IEEE Trans. Ind. Appl.*, vol. IA-22, no. 5, pp. 820–827, 1986. doi: 10.1109/TIA.1986.4504799.

[17] M. Depenbrock, "Direct self-control (DSC) of inverter-fed induction machine," *IEEE Trans. Power Electron.*, vol. 3, no. 4, pp. 420–429, 1988. doi: 10.1109/63.17963.

[18] T. G. Habetler, F. Profumo, M. Pastorelli, and L. M. Tolbert, "Direct torque control of induction machines using space vector modulation," *IEEE Trans. Ind. Appl.*, vol. 28, no. 5, pp. 1045–1053, 1992. doi: 10.1109/28.158828.

[19] J.-K. Kang and S.-K. Sul, "New direct torque control of induction motor for minimum torque ripple and constant switching frequency," *IEEE Trans. Ind. Appl.*, vol. 35, no. 5, pp. 1076–1082, 1999.

[20] T. Noguchi, H. Tomiki, S. Kondo, and I. Takahashi, "Direct power control of PWM converter without power-source voltage sensors," *IEEE Trans. Ind. Appl.*, vol. 34, no. 3, pp. 473–479, 1998. doi: 10.1109/28.673716.

[21] G. Escobar, A. M. Stankovic, J. M. Carrasco, E. Galván, and R. Ortega, "Analysis and design of direct power control (DPC) for a three phase synchronous rectifier via output regulation subspaces," *IEEE Trans. Power Electron.*, vol. 18, no. 3, pp. 823–830, 2003. doi: 10.1109/TPEL.2003.810862.

[22] S. S. Lee and Y. E. Heng, "Table-based DPC for grid connected VSC under unbalanced and distorted grid voltages: Review and optimal method," *Renew. Sustain. Energy Rev.*, vol. 76, pp. 51–61, 2017. doi: 10.1016/j.rser.2017.03.033.

[23] M. Malinowski, M. Jasiński, and M. P. Kazmierkowski, "Simple direct power control of three-phase PWM rectifier using space-vector modulation (DPC-SVM)," *IEEE Trans. Ind. Electron.*, vol. 51, no. 2, pp. 447–454, 2004. doi: 10.1109/TIE.2004.825278.

[24] D. Zhi, L. Xu, and B. W. Williams, "Improved direct power control of grid-connected dc/ac converters," *IEEE Trans. Power Electron.*, vol. 24, no. 5, pp. 1280–1292, 2009. doi: 10.1109/TPEL.2009.2012497.

[25] J. Hu, L. Shang, Y. He, and Z. Zhu, "Direct active and reactive power regulation of grid-connected dc/ac converters using sliding mode control approach," *IEEE Trans. Power Electron.*, vol. 26, no. 1, pp. 210–222, 2011. doi: 10.1109/TPEL.2010.2057518.

[26] Y. Gui, G. H. Lee, C. Kim, and C. C. Chung, "Direct power control of grid connected voltage source inverters using port-controlled Hamiltonian system," *Int. J. Control Automation Syst.*, vol. 15, no. 5, pp. 2053–2062, 2017. doi: 10.1007/s12555-016-0521-9.

[27] S. Vazquez et al., "Model predictive control: A review of its applications in power electronics," *IEEE Ind. Electron. Mag.*, vol. 8, no. 1, pp. 16–31, 2014. doi: 10.1109/MIE.2013.2290138.

[28] D.-K. Choi and K.-B. Lee, "Dynamic performance improvement of ac/dc converter using model predictive direct power control with finite control set," *IEEE Trans. Ind. Electron.*, vol. 62, no. 2, pp. 757–767, 2015. doi: 10.1109/TIE.2014.2352214.

[29] J. Hu, "Improved dead-beat predictive DPC strategy of grid-connected dc–ac converters with switching loss minimization and delay compensations," *IEEE Trans. Ind. Informat.*, vol. 9, no. 2, pp. 728–738, 2013. doi: 10.1109/TII.2012.2223705.

[30] Y. Gui, C. Kim, and C. C. Chung, "Grid voltage modulated direct power control for grid connected voltage source inverters," in *Proc. American Control Conf.*, pp. 2078–2084, 2017.

[31] Y. Gui, M. Li, J. Lu, S. Golestan, J. M. Guerrero, and J. C. Vasquez, "A voltage modulated DPC approach for three-phase PWM rectifier," *IEEE Trans. Ind. Electron.*, vol. 65, no. 10, pp. 7612–7619, Oct. 2018. doi: 10.1109/TIE.2018.2801841.

[32] Y. Gui, X. Wang, and F. Blaabjerg, "Vector current control derived from direct power control for grid-connected inverters," *IEEE Trans. Power Electron.*, to be published. doi: 10.1109/TPEL.2018.2883507.

[33] P. Kundur, N. J. Balu, and M. G. Lauby, *Power System Stability and Control*, vol. 7. New York: McGraw-Hill, 1994.

[34] F. Z. Peng and J.-S. Lai, "Generalized instantaneous reactive power theory for three-phase power systems," *IEEE Trans. Instrum. Meas.*, vol. 45, no. 1, pp. 293–297, 1996.

[35] B. K. Bose, *Power Electronics AC Drives*. Englewood Cliffs, NJ: Prentice Hall, 1986.

[36] K. Ogata and Y. Yang, *Modern Control Engineering*. Englewood Cliffs, NJ: Prentice-Hall, 1970.

[37] Y. Gui, C. Kim, C. C. Chung, J. M. Guerrero, Y. Guan, and J. C. Vasquez, "Improved direct power control for grid-connected voltage source converters," *IEEE Trans. Ind. Electron.*, vol. 65, no. 10, pp. 8041–8051, Oct. 2018.

[38] S. Buso and P. Mattavelli, *Digital control power electronics*, 2nd ed. Morgan & Claypool Publishers, 2015. doi: 10.2200/S00637ED1V01Y201503PEL007.

[39] D. Holmes, T. Lipo, B. McGrath, and W. Kong, "Optimized design of stationary frame three phase AC current regulators," *IEEE Trans. Power Electron.*, vol. 24, no. 11, pp. 2417–2426, 2009. doi: 10.1109/TPEL.2009.2029548.

[40] D. Pan, X. Ruan, X. Wang, H. Yu, and Z. Xing, "Analysis and design of current control schemes for LCL-type grid-connected inverter based on a general mathematical model," *IEEE Trans. Power Electron.*, vol. 32, no. 6, pp. 4395–4410, 2017. doi: 10.1109/TPEL.2016.2602219.

[41] B. Wei, Y. Gui, A. Marzabal, S. Trujillo, J. M. Guerrero, and J. C. Vasquez, "Distributed average secondary control for modular UPS systems based microgrids," *IEEE Trans. Power Electron*, 2018, to be published. doi: 10.1109/TPEL.2018.2873793.

[42] J. Svensson, "Synchronisation methods for grid-connected voltage source converters," in *Proc. IET Generation Transmission and Distribution*, vol. 148, no. 3, pp. 229–235, 2001. doi: 10.1049/ip-gtd:20010101.